Facile Fabrication of Spherical Architecture of Ni/Al Layered Double Hydroxide Based on *In Situ* Transformation Mechanism

Fazhi Zhang, Yue Zhang, Caili Yue, Rong Zhang, and Yanmin Yang
State Key Laboratory of Chemical Resource Engineering, Beijing University of Chemical Technology, Beijing 100029, China

DOI 10.1002/aic.14609
Published online September 16, 2014 in Wiley Online Library (wileyonlinelibrary.com)

Spherical architectures of nickel–aluminum layered double hydroxide (NiAl-LDH) with hydrotalcite-like nanoflakes as building blocks were facilely fabricated by precipitation reaction in aqueous solution without any surfactants and organic solvents. Growth of such unique structure undergoes preorganization of primary nanospheres of colloidal amorphous aluminum hydroxide (AAH) in solution, followed by nucleation and crystallizaion of LDH from exterior to interior of AAH spheres by an in situ transformation mechanism. The structure and morphology of LDH spheres depend on both starting raw materials and synthetic parameters including reaction time, reaction temperature, and aqueous ammonia dosage. NiAl-LDH sphere as positive electrode material delivers improved rechargeable and discharge capacity, with the highest discharge capacity of 173 mAh g^{-1} at a current density of 30 mA g^{-1} within a potential range from −0.1 to 0.45 V in 10 mol L^{-1} KOH solution, due to the faster diffusion processes in the spherical architecture than the powder sample. © 2014 American Institute of Chemical Engineers *AIChE J*, 60: 4027–4036, 2014
Keywords: spherical architecture, layered double hydroxide, electrochemical property, electrode material, in situ transformation

Introduction

Integration of nanosized materials into higher ordered architectures is of great importance in developing new functional devices for practical applications.[1–5] Porous nanosphere as one of three-dimensional (3-D) assembled structures from low-dimensional building blocks such as nanoparticles, nanorods, and nanosheets can provide nanomaterials with high specific surface areas, strong mechanical strengths, and fast mass and electron transport kinetics. These 3-D spherical architectures have shown specific functions in a large variety of research fields such as high-performance structural and functional devices, chemo- and biosensors, catalysts, adsorbents, energy conversion, and biomedical materials.[5–8] Various fabrication strategies have been attempted for the integration of nanomaterial into 3-D architectures over the last two decades, such as self-organization,[1–3] field-,[9,10] bio-,[11] and interface-directed[12] techniques, however, disadvantages related to complicated fabrication procedures, high cost, and environmental contamination have hindered the further scale up of many of these methods for large scale applications successfully. In this sense, the development of simple, environmentally benign, and controllable assembly technologies remain a challenge for the actual practical applications. Layered crystal materials are a special type of compounds in which the crystals are built by stacking of two-dimensional (2-D) units connected to each other through weak interactions such as van der Waals, electrostatic, and coulombic forces.[13] Among the layered materials, a class of anionic clays: layered double hydroxides (LDHs, also known as hydrotalcite-like materials) have been paid much attention recently, due to their potential industrial applications as adsorbing/separating agents, additives in polymers, and precursors for catalysts, semiconductors, electrical, magnetic and optical materials.[14–18] Assembling such 2-D platelets into organized 3-D architectures would be indispensable and significant for further applications of the layered crystals materials by tuning and controlling their electrical, optical, mechanical, or chemical properties.

Recently, fabrication of LDHs with 3-D architectures has been reported by the surfactants-assisted process in hydro/solvothermal reaction mixtures.[19–24] For example, coral-like porous MgAl-LDH microspheres have been synthesized in a nonaqueous polar solvent/surfactant system of ethylene glycol/methanol/dodecyl sulfate.[19] In subsequent cases, sodium dodecanesulfonate,[20] glycine,[21] sodium alginate,[22] cetyltrimethyl ammonium bromide,[23] and sodium dodecyl sulfonate[24] have been applied as soft templates in this field. In those studies, uniform LDH nanocrystals are suggested to be first attained on nucleation and crystallization in the surfactants-assisted process. Subsequently, the formed nanocrystals will assemble into microspheres in order to

Additional Supporting Information may be found in the online version of this article.

Correspondence concerning this article should be addressed to F. Zhang at zhangfz@mail.buct.edu.cn

minimize the surface energy during the solvothermal treatment. However, the size of the as-prepared 3-D LDH architectures is usually at micrometer range. It is noted that nanosized assembly is not easy to be acquired in the case of LDH for the chemical bonds are not isotropic in 3-D orientation. Furthermore, such attempted approaches with organic surfactants and solvents often require dealing with a lot of organic solvent, which is neither convenient nor environmental friendly. Thus, the developing of surfactant-free approach for nanosphere architectures of LDH working under mild conditions is highly desired. Herein, we report a simple and effective fabrication of 3-D nickel–aluminum layered double hydroxide (NiAl-LDH) spherical architecture by *in situ* transformation of preorganized primary amorphous aluminum hydroxide (AAH) nanospheres in solution containing basic aluminum acetate (BAA), nickel acetate, and aqueous ammonia, without using any surfactants and organic solvents. The formation course, such as the evolution of phase composition, structure, and particle morphology during the whole process is verified and the mechanism of LDH sphere formation is postulated based on the characterization results. Detailed investigations of starting raw materials and synthetic parameters including reaction time, reaction temperature, and aqueous ammonia dosage are further carried out for control of structure and morphology of LDH spheres.

Rechargeable batteries are becoming more and more important in everyday life, especially in consumer electronic devices and city transportation.[25,26] The prospect of developing high-performance nickel hydroxide-positive electrodes for application in various nickel-based rechargeable alkaline storage cells is an exciting direction in the field of electrical energy storage. Introducing bi- or trivalent cations, such as Co^{2+}, Zn^{2+}, Al^{3+}, Mn^{3+}, and Fe^{3+}, into the nickel hydroxide lattice has been reported to have a greater discharge capacity and higher utilization of active material than the β-$Ni(OH)_2$ electrode, which might be related to the stable lamellar structure, efficient water relay system to make rapid anion migration, and the effects of interlayer anions.[15,27–30] The aggregation of active material tends to reduce the accessible surface area for participating electrochemical reaction and the utilization ratio of the active material. Thus, the fabrication of electrode materials with higher and more accessible surface area plays a key role in the development of energy storage technology.[30–32] For example, hollow structure of the nickel hydroxide tube was revealed to contribute to superior capacity, reversibility, high rate discharge, high-temperature performance, and cycling stability compared with dense spherical powder sample.[32] With this in mind, the electrochemical performance of the obtained NiAl-LDH spherical architecture is further tested as an example of its practical applications, which exhibits improved rechargeable and discharge capacity compared with NiAl-LDH powder sample. The approach we presented is simple and environmentally benign, and accessible to scale up for fabrication of 3-D LDH architectures, which proves good application prospect in energy storage and conversion devices.

Experimental Section

Synthesis of LDH spherical architectures

All the reagents were analytical grade and used without further purification. NiAl-LDH spherical architectures were fabricated by precipitation reaction in aqueous solution containing BAA, nickel acetate, and aqueous ammonia. In a typical synthesis, $Al(OH)(OCOCH_3)_2{\cdot}2H_2O$ (1.6 mmol) was added to an aqueous solution of $Ni(OCOCH_3)_2{\cdot}4H_2O$ (80 mL, with $[Ni^{2+} + Al^{3+}] = 0.1$ mol L^{-1} and Ni^{2+}/Al^{3+} molar ratio = 4) in a three-neck flask which was soaked in a water bath previously heated to 60°C under continuous stirring. A suspension of BAA particles was obtained. Then, aqueous ammonia (15 mL, 28 wt %) was added quickly and the color of suspension was changed from light green to deep blue immediately, accompanying the further dissolution of BAA particles. The initial reaction time was recorded as 0 min after adding aqueous ammonia. After reaction, the precipitate was filtered off, washed repeatedly with deionized water and anhydrous ethanol. The washed specimens were dried in an oven at 60°C overnight.

Other experiment was undertaken in which the aqueous ammonia dosage was altered from 5 to 40 mL. The reaction temperature and duration of the reaction were varied between 50 and 90°C and 0.5 min to 24 h, respectively. For comparison, $Ni(NO_3)_2$ and $Al(NO_3)_3$ were also used as Ni and Al precursor, respectively, and urea was used as basic precipitator instead of ammonia aqueous solution. Moreover, the hydrolysis of $Al(OH)(OCOCH_3)_2{\cdot}2H_2O$ with ammonia aqueous solution under the same conditions but in the absence of $Ni(OCOCH_3)_2.4H_2O$ were undertaken.

Material characterization

Powder x-ray diffraction (XRD) patterns of the samples were collected on a Shimadzu XRD-6000 diffractometer using a Cu Kα source, with a scan step of 0.02° and a scan range between 3° and 70°. Fourier transform infrared (FTIR) spectrum was recorded in the region 4000–400 cm^{-1} on a Bruker Vector 22 spectrometer using KBr pellet technique. The morphologies of the samples were investigated using a scanning electron microscopy (SEM) instrument (Zeiss SUPRA 55) with an accelerating voltage of 20 kV. Transmission electron microscopy (TEM) and high-resolution transmission electron microscope (HRTEM) images were recorded with JEOL JEM-2010 transmission electron microscope. The accelerating voltage was 200 kV in each case. The specific surface area determination and size analysis were performed by Brunauer–Emmett–Teller (BET) and Barrett–Joyner–Halenda (BJH) method, respectively, using a Micromeritics ASAP 2020 analyzer. Prior to the measurement, the samples were degassed at 100°C for 6 h. X-ray photoelectron spectrometer (XPS) measurements were recorded on an ESCALAB 250 XPS, operating at a typical pressure of about 2×10^{-9} Pa using Al Kα x-rays as the excitation source (1486.6 kV) in 0.05 eV energy step size.

Electrochemical characterization

Electrochemical characterizations were performed in a three-compartment electrolysis cell, in which a piece of Ni foam was used as the counter electrode and an Hg/HgO electrode as the reference electrode.[29] Cyclic voltammetric studies were carried out on a electrochemical workstation (CS350, Corrtest, China) at room temperature. Cyclic voltammetry measurements were conducted at a scan rate of 0.5 mV s^{-1} vs. Hg/HgO. Galvanostatic charge–discharge studies were conducted on a LAND CT2001A cell performance tester. After the working electrode had been immersed in a 10 mol L^{-1} KOH solution for 24 h, the electrode was charged for at a current density of 30 mA g^{-1} and

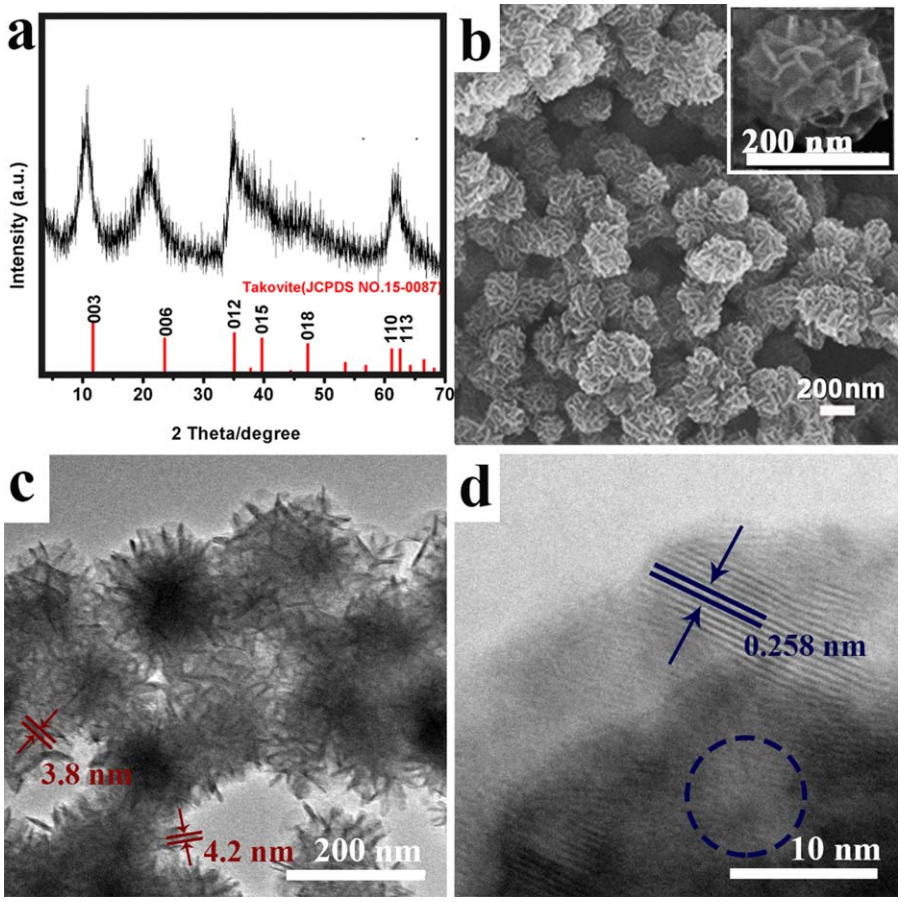

Figure 1. XRD pattern (a) and SEM (b), TEM (c), and HRTEM (d) images of LDH spherical architecture obtained at 60°C for 12 h with aqueous ammonia dosage 15 mL.

XRD pattern of takovite crystal (JCPDS No.15–0087) is included for comparison. Insets of (b) show the high-magnification SEM images of a represented individual architecture. [Color figure can be viewed in the online issue, which is available at wileyonlinelibrary.com.]

discharged at the same density until the potential was −1 V. Herein, the current densities and discharge capacities per gram were all calculated according to the weight of LDH used in the preparation of the electrode.

Results and Discussion

NiAl-LDH spherical architecture was fabricated by the precipitation reaction in mixtures containing BAA aqueous suspension and nickel acetate solution with ammonia aqueous solution as alkali source. The crystal phase of the resulting sample produced at 60°C for 12 h was analyzed by XRD (Figure 1a), which exhibits a series of (*00l*) diffraction lines at low 2θ values, characteristic of a layered structure. The diffraction lines are similar to those of takovite crystal (JCPDS No. 15–0087, a kind of hydrotalcite-type material with carbonate ions intercalated into gallery). The (003) peak appears at 10.5° (the interlayer spacing d_{003} = 0.85 nm), demonstrating the intercalation of acetate anions into LDH gallery.[33,34] Figure 1a also shows the emergence of two broad asymmetric peaks around 35.2° and 62.2° corresponding to (012) and (110)/(113) reflection line, respectively, confirming a hexagonal lattice with a 3R stacking of LDH layers.[35]

Figure 1b shows a typical SEM image of the production composed by the spherical architectures leading to a nondensely packed arrangement. The size of the spherical forms is in the range of 150–200 nm. SEM image at a high-magnification (inside of Figure 1b) reveals the morphology of an individual sphere-like architecture which consists of dozens of nanoflakes intercrossed with each other. The spherical morphology and interior feature of the LDH architectures is further confirmed by TEM observation (Figure 1c). Well-defined spheres with size about 200 nm are observed. LDH nanosheets with platelet edge length in the range of 30–60 nm and thickness about 4 nm appear as needles. Such an extrinsic feature is due to the vertical orientation of the LDH primary nanosheets to the Cu grid when stacking to form the sphere. HRTEM image provides further evidence of the appearance of LDH crystalline phase (Figure 1d), which demonstrates the lattice fringes of (012) plane with a lattice gap of 0.258 nm. Also, we observe the ill-defined lattice fringes designated by blue dotted circle suggesting the weak crystallinity in this region.

The intercalation of acetate anions into interlayer region of LDHs can be further confirmed by FTIR spectroscopy (Figure 2). The broad band at about 3645 cm^{-1} is characteristic peak of the stretching vibration of hydroxyl groups in the lattice of LDHs hydrogen-bonded to H_2O molecule and anion interlayer. The asymmetric and symmetric carbonyl vibration bands of acetate, respectively, at 1645 and

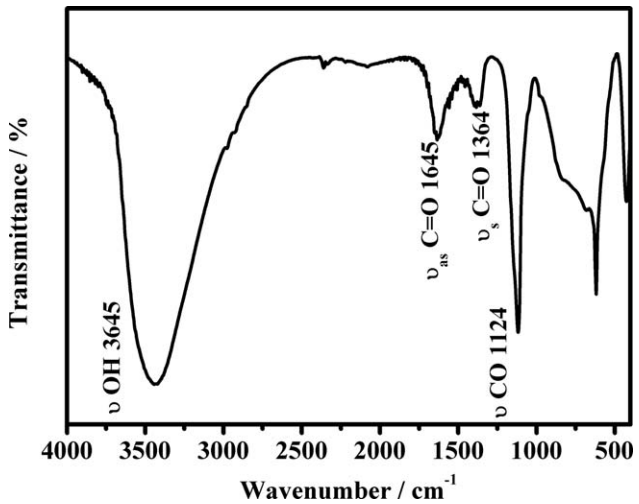

Figure 2. FTIR spectrum of LDH spherical architecture obtained at 60°C for 12 h with aqueous ammonia dosage 15 mL.

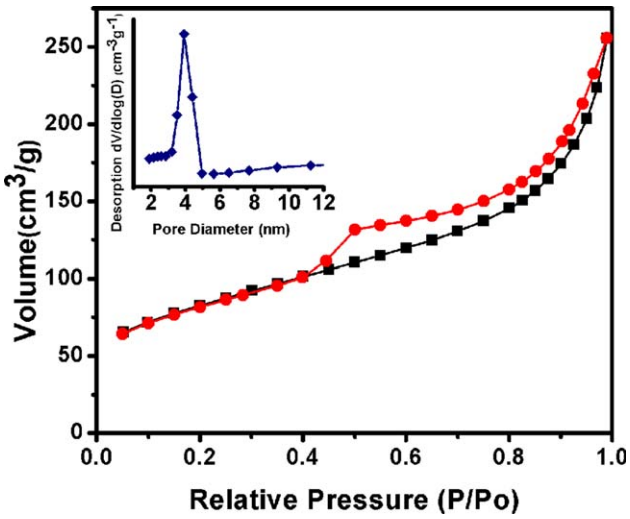

Figure 3. N_2-sorption isotherm and pore-size distribution (inset) of LDH spherical architecture obtained at 60°C for 12 h with aqueous ammonia dosage 15 mL.

[Color figure can be viewed in the online issue, which is available at wileyonlinelibrary.com.]

1364 cm^{-1} are observed, along with the stretching vibration of C—O at 1124 cm^{-1}.[34]

We can see from Figure 3 that the adsorption isotherm of LDH spherical architecture displays a type-IV characteristic with a H3-type hysteretic loop at the relative pressure ($p/p_0 > 0.4$), indicating the presence of a mesoporous structure. The BET specific surface area is calculated to be 284 $m^2 g^{-1}$. The relatively larger specific surface area may be attributed to the LDH architecture structure with a large amount of hierarchical pores which will give great contribution to the surface area when the particle sizes are in the nanometer scale.[36] The pore-size distribution of the LDH sphere calculated by BJH method from desorption branch (inset of Figure 3) exhibits a narrow size distribution around 3–5 nm.

With the aim of controlling effectively the morphology of 3-D LDH spherical architectures and further allow the properties to be tailored to specific applications, a detailed understanding of the mechanism of architectures formation was carried out in this article. Figure 4a shows an accumulation of BAA particles with multifarious shapes. The BAA particles are insoluble after adding to an aqueous solution of nickel acetate at 60°C under continuous stirring. However, adding ammonia aqueous solution to the suspension for 0.5 min can lead to the disintegrating of the BAA bulk and a compact aggregation of spherical particles with the size about 100–150 nm is formed (Figure 4b). Individual orbicular particles cannot be distinguished anymore. Meanwhile, XRD pattern illustrates that the characteristic reflections of BAA (Figure 5; JCPDS No. 13-0833) have completely disappeared for the sample with reaction time 0.5 min (Figure 5a). Instead, we can observe weak LDH diffraction peaks begin to appear with broad diffuse peaks below 40° characteristic of amorphous phase which maybe AAH gel.[37] It is interesting to see numerous distinguished nanoflakes curve from the surface of spherical particles after reaction time 1 min (Figure 4c). Consequently, an obvious increasing intensity of LDH diffraction peaks at 10.5° and 21.1° has been showed for the sample obtained with reaction time from 0.5 to 3 min (Figure 5b), indicating the forming of LDH crystals on the particle surface and the intercalation of acetate into the LDH gallery. With extended reaction time for 8 h (Figure 4e), individual rounded particles with numbers of LDH nanoflakes interlaced on the surface can be identified. XRD patterns also demonstrate a pronounced raise of the intensity of (003) reflection peak of LDH structure (Figure 5c). When the duration of reaction was further prolonged, the size of LDH architecture enlarges from 100–150 nm (reaction time 8 h, Figure 4e) to 150–200 nm (reaction time 12 h, Figure 1b). It is noted that the particle size does not increase with the reaction time 24 h (Figure 4f), but the (003) reflection intensity strengthens further (Figure 5e), indicating a gradual crystallization of LDH platelets.

The above SEM and XRD results denote the formed AAH spherical particles during the initial stage of reaction may induce the construction of 3-D LDH architectures with the used synthesis conditions. An additional experiment to further verify the formation and evolution process of the solid reaction intermediates AAH within ammonia aqueous solution was carried out. The experiment was conducted using only BAA and ammonia aqueous solution as raw materials at 60°C. The SEM images of samples taken at different stirring times are shown in Supporting Information Figure S1. Congregated spherical particles with size about 100–150 nm are immediately formed on adding ammonia aqueous solution for a short time 0.5 min (Supporting Information Figure S1a). XRD shows broad diffuse peak attributed to the AAH phase for the sample at the early stage (Supporting Information Figures S2a, b). The following hydrolysis reaction (Eq. 1) for BAA may occur within the ammonia aqueous solution

$$Al(OH)(OCOCH_3)_2(s) + H_2O \leftrightarrows Al(OH)_3(s) + H^+ + CH_3COO^- \quad (1)$$

It is noted that the spherical nanoparticles of sample obtained after reaction 1 min (Supporting Information Figure S1b) show a smaller particle size than those after 0.5 min, which may be due to the dissolving of the AAH particles in the alkaline solutions (Eqs. 2 and 3)

$$Al(OH)_3(s) \leftrightarrows Al(OH)_2{}^+ + OH^- \leftrightarrows Al(OH)^{2+} + OH^- \leftrightarrows Al^{3+} + OH^- \quad (2)$$

or

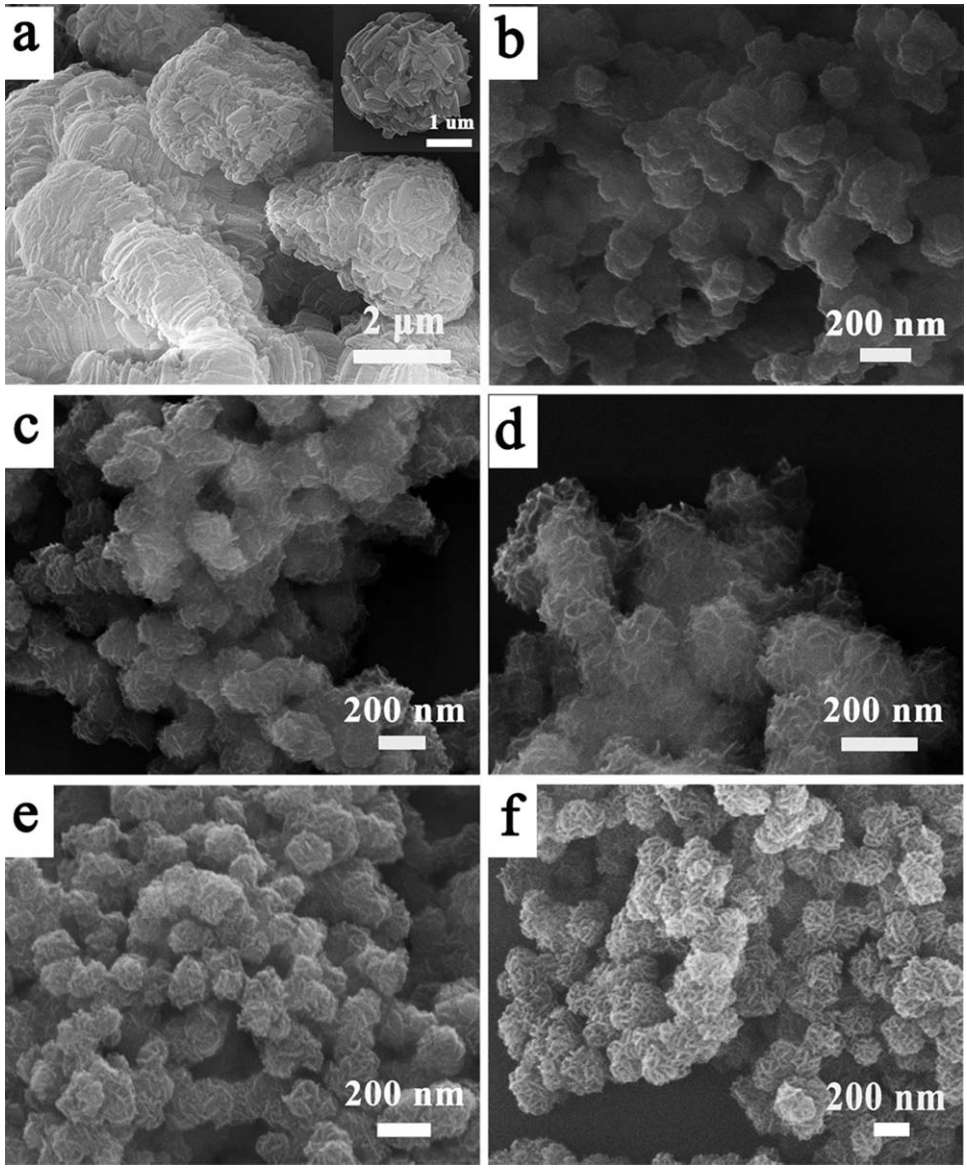

Figure 4. SEM images of reagent BAA (a) and LDH spherical architectures obtained with different reaction times: 0.5 min (b), 1 min (c), 3 min (d), 8 h (e), and 24 h (f) at 60°C with aqueous ammonia dosage 15 mL.

$$Al(OH)_3(s)+OH^- \leftrightarrows Al(OH)_4^- \quad (3)$$

With the reaction time of 10 min, the spherical aggregates of AAH collapse to form the alveolate-like particles (Supporting Information Figure S1c). Meanwhile, weak diffraction peaks of boehmite can be detected (JCPDS No. 83-2384; Supporting Information Figure S2c). The diffraction intensity of boehmite strengthens for the sample obtained after reaction 24 h (Supporting Information Figure S2d). The above SEM and XRD observation demonstrate that AAH phase can be formed during the early stage within ammonia aqueous solution. Crystallization of boehmite may occur with a prolonged reaction time. As the acetate ions from hydrolysis of BAA can link to aluminum atom on AAH, probably by mononuclear outer-sphere complexes, that is, complex which are coordinated to OH— groups and/or water molecules at the hydrated surface through electrostatic interactions and hydrogen bonding,[38] AAH tends to form nanoparticle agglomerates with external spherical appearance in aqueous solution to decrease the total system energy. For estimating the important role of the acetate ions for the controlling of the formation of LDH spherical architectures, an additional experiment was performed using $Al(NO_3)_3$ and $Ni(NO_3)_2$ as the Al and Ni precursor salt, respectively. Only round-like particles with size about 30 nm can be obtained (Supporting Information Figure S3a). In fact, even with BAA and $Ni(NO_3)_2$ as raw materials, we cannot obtain the LDH spherical architecture (Supporting Information Figure S3b). It is concluded that the appropriate quantity of acetate ions is necessary for bonding the $Al(OH)_3$ to AAH orbicular agglomerates, which further induce the construction of LDH spherical architecture.

According to the literatures, chemically induced self-transformation process from the aggregated precursor particles with globular shape has been performed by several groups as one of the nontemplate methods for fabrication of hollow inorganic materials.[39–42] Several mono-metal compounds such as hollow spheres of SnO_2,[39] $CaCO_3$,[40] WO_3,[41] and γ-AlOOH[42] have been fabricated through the self-transformation process. In our case, the crystallization

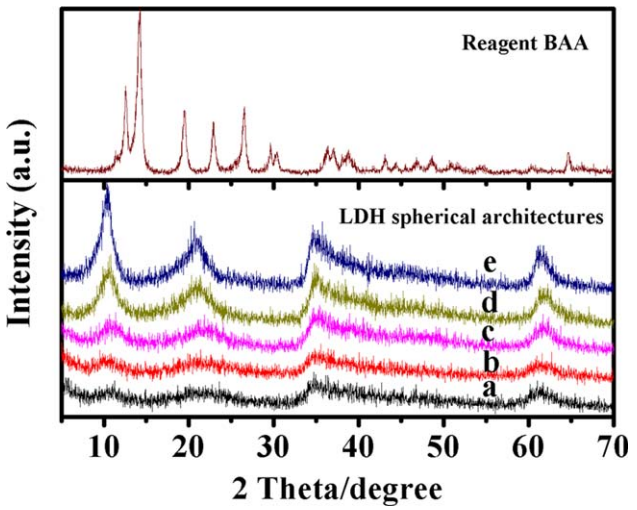

Figure 5. XRD patterns of reagent BAA and LDH spherical architectures obtained with different reaction time: 0.5 min (a), 3 min (b), 8 h (c), 10 h (d), and 24 h (e) at 60°C with aqueous ammonia dosage 15 mL.

[Color figure can be viewed in the online issue, which is available at wileyonlinelibrary.com.]

process of LDH spherical architecture is relatively complicated in consideration of the double metal hydroxides system. The observation of the evolution process of BAA in the ammonia aqueous solution illustrates a behavior of BAA hydrolysis to AAH orbicular agglomerates and subsequent recrystallization to boehmite (Supporting Information Figure S1 and Figure 2). Moreover, the dissolved $Al(OH)_4^-$ species may have great opportunity to react with abundant Ni^{2+} ions to nucleate inside the reaction solution, leading to the formation of discrete LDH crystalline. Herein, these problems can be mitigated by the complex formation of Ni^{2+} with a large excess of ammonia in solution (Eq. 4)

$$Ni^{2+} + NH_3 \leftrightarrows Ni(NH_3)_6^{2+} \tag{4}$$

Actually, we observe an obvious change of the solution color from light green to deep blue with the addition of ammonia aqueous solution, demonstrating the initiation of the complexing reaction. We suggest that the formed $Ni(NH_3)_6^{2+}$ complex provide a feasible period for preorganization of AAH spheres and prevent the direct nucleation of NiAl-LDH in the solution. Experimentally, when we replaced ammonia aqueous solution with urea for fabrication of LDH architecture, only partially collapsed or irregularly shaped microspheres with the size above 4 μm are obtained (Supporting Information Figure S4a). Because the thermal activation of urea decomposition at ambient pressure requires a long reaction time, the releasing rate of Al^{3+} species is relatively slow when using urea as precipitator. Thereby, the LDH nucleation and crystal growth take a comparatively long time, leading to a larger spherical form. Moreover, when using strong base NaOH as the basic precipitator (Supporting Information Figure S4b), the obtained products are not organized architectures but discrete nanoplates with a diameter size about 30 nm. We speculate that the increasing pH of reaction solution with NaOH makes the solid $Al(OH)_3$ dissolving rapidly into $Al(OH)_4^-$, and thus LDH nuclei form in the solution instead of on the surface of AAH spheres.

XPS spectra of Al 2p and Ni 2p for the specimens obtained with different reaction times were given in Supporting Information Figure S5. We can recognize that the spectrum of Al 2p for the specimen prepared with reaction time 0.5 min shows a peak with binding energy of 75.0 eV, related to the Al^{3+} species in the form of Al−OH of the amorphous phase (Supporting Information Figure S5a).[43] With prolonging the reaction time, the peak at 75.0 eV gradually disappears, and simultaneously another peak at 74.1 eV, which may be attributed to the Al^{3+} species in NiAl-LDH,[44] shifts to 74.4 eV. A positive shift of Al 2p signal for the Al^{3+} species in the AAH phase indicates that the electron cloud density surrounding the aluminum nuclei may be decreased accompanying the formation of LDH phase by incorporation of Ni^{2+} with aluminum hydroxide in the layer. In addition, XPS spectra of Ni 2p exhibit two peaks at 856.2 and 862.3 eV for all the specimens, which may be associated with the Ni^{2+} species in NiAl-LDH.[44]

On the basis of above systematic experimental results, we propose a schematic formation mechanism of LDH spherical architecture via the template-free *in situ* transformation process, as represented in Figure 6. After adding ammonia aqueous solution into the reaction mixtures containing BAA aqueous suspension and nickel acetate solution, BAA hydrolysis takes place rapidly in the basic solution, leading to the disintegration of the bulk to a compact aggregation of AAH spherical nanoparticles (Eq. 1). This preorganized AAH spheres could be an important stage for the assembled morphology controlling of the final LDH spherical configuration. Hydrolysis of BAA in ammonia aqueous solution can produce plenty of acetate ions, which may form one dominating outer-sphere surface complex on water-aluminum hydroxide interface, along with those from reagent nickel acetate. Thus, AAH tends to form spherical nanoparticle agglomerates in the aqueous solution by decreasing the surface tension. It is worth noting that the complexing of acetate may slow down the dissolving of the solid AAH which contributes to the construction of 3-D spherical architectures (discussed below). Moreover, we suggest that in order to prevent the direct nucleation of NiAl-LDH in the solution, the complexing reaction between Ni^{2+} and a large excess of NH_3 (Eq. 4) provide a feasible period for preorganization of AAH spheres from BAA compound. Then, the formed $Ni(NH_3)_6^{2+}$ complexes may be adsorbed on the exterior surface of AAH spheres (Step 1).

Subsequently, the surface-absorbed Ni^{2+} from the dissociation of $Ni(NH_3)_6^{2+}$ complexing compounds in the alkaline solution (Eq. 4) incorporate with aluminum compounds on the AAH surface and positively charged brucite-like sheets form using the distinct NiO_6 and AlO_6 octahedral with plenty of surface-located OH— groups, which should easily attract the negatively charged acetate groups via electrostatic interaction. Then, the stacking of sheets begins to form layered structure with the participation of hydroxide anion (OH^-), acetate, and water, resulting in the LDH nucleation (Eq. 5, Step 2)

$$Ni^{2+} + Al(OH)_3(s) + OH^- + H_2O + CH_3COO^- \leftrightarrows NiAl-LDH(CH_3COO^-)(s) \tag{5}$$

In the next stage, LDH nuclei adhered on the surface of preorganization AAH spheres are *in situ* crystallized in the basic solution (Step 3). We suggest that the continuous dissociation of the $Ni(NH_3)_6^{2+}$ complexing compound and the

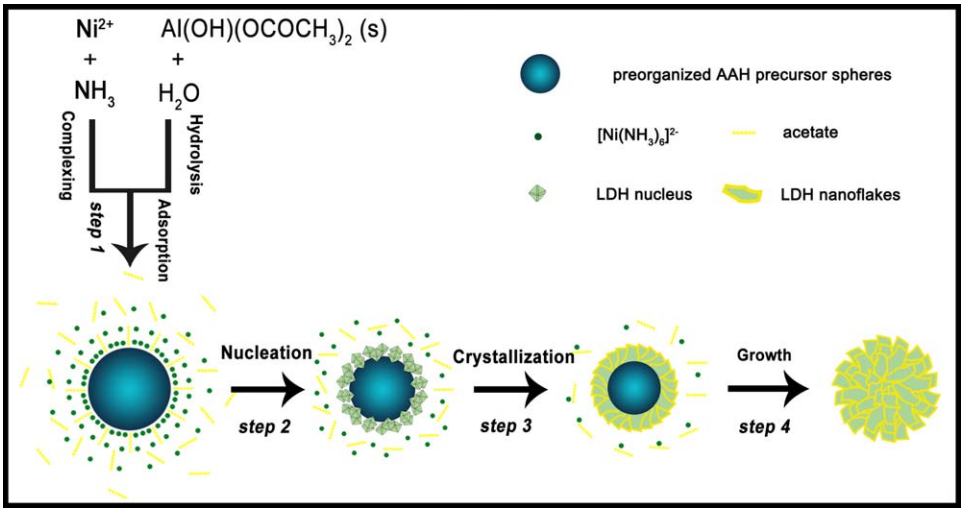

Figure 6. Schematic illustration of a proposed evolution process of NiAl-LDH spherical architectures.

***Step 1: Preorganization of AAH precursor spheres from reagent BAA with $Ni(NH_3)_6^{2+}$ complexes adsorbed on the exterior surface. Step 2: Conversion of Ni^{2+} and Al^{3+} species to form NiAl-LDH nuclei, with the participation of hydroxide anion, acetate, and water. Step 3: LDH phase is *in situ* crystallized on the surface of the preorganized AAH spheres; crystallization proceeds toward the AAH interior until the crystals eventually bond with the sphere. Step 4: Extended crystallization time results in stable LDH spherical architecture which consists of dozens of nanoflakes intercrossed with each other; an "evolution selection mechanism" is suggested to be responsible for the inward growth orientation and interlaced accumulation of the LDH nanoplates with abundant channels. [Color figure can be viewed in the online issue, which is available at wileyonlinelibrary.com.]**

preorganized AAH material supply the necessary nutrients for the crystallization and growth of LDH nanoplatelets. According to literature, the release of Al^{3+} cations from alumina can be improved by adsorption of cations such as Ni^{2+} and Zn^{2+}.[45] It is aware of the mass relocation starting from the AAH surface region. As a result, LDH phase crystallization proceeds toward the AAH phase interior until the crystals eventually bond with the sphere. For an anisotropic LDH crystallite, growth in the *ab*-direction is obviously faster than that in the *c*-direction, ensuring that crystals with their fastest growth direction normal to the AAH surface eventually envelop all the other crystals. Accordingly, the interlaced accumulation of LDH platelets restricts the growth by each other, giving a final spherical conformation composed of nanoflakes with abundant channels. The gradual increase in the intensity of basal reflection illuminates that the crystallization degree of LDH increases with extended reaction time, resulting in a stable spherical aggregation finally (Step 4).

In brief, the formation process of the 3-D LDH spherical architecture is likely to be the result of preorganization of AAH sphere particles in ammonia aqueous solution, complexing between Ni^{2+} and NH_3 and deposition the production $Ni(NH_3)_6^{2+}$ compounds on the AAH surface, conversion of Ni^{2+} and aluminium species to NiAl-LDH nuclei, *in situ* crystallization and growth of LDH from the exterior to the interior of AAH spheres. The compromise among the above involved chemical reactions may be possible to dominate the development of the LDH architectures. It is noted that several key problems need to be overcome in this case. First, the preorganization of AAH spheres is an essential prerequisite for inducing the construction of LDH architectures. Many aluminum salts are soluble in water and the intermediate amorphous phases obtained from hydrolysis are often in the form of gels or irregularly shaped aggregates of nanoparticles rather than discrete and morphologically distinct particles. In the present study, the adoption of BAA as raw material could produce spherical AAH particles possibly by decreasing the surface tension through the formation of mononuclear outer-sphere complexes between acetate ions and aluminum species on the water-aluminum hydroxide interface.[38] Second, the preorganized AAH spheres tend to crystallize to form boehimite phase in the basic aqueous solution such that the amorphous phases are extremely short-lived. It is worth noting that ammonia aqueous solution as reagent in the reaction mixtures can work as both precipitant and complexing agent. The strongly complexing reaction between Ni^{2+} and a large excess of NH_3 may prevent the direct nucleation of LDH in the solution and provide a feasible period for the preorganization of metastable AAH sphere agglomerates from BAA compound. Third, the relative rate of dissolution of the intermediate AAH particles should be assorted with that of nucleation of LDH. When the former is relatively fast, the amorphous phase will completely dissolve prior to crystallization, leading to the formation of discrete LDH phase in the free solution. Only when the rates are well-matched will the amorphous particles *in situ* transform to the LDH crystalline nanospheres.

Further research of synthetic parameters such as reaction temperature and aqueous ammonia dosage on the control of the structure and morphology of the obtained LDH spherical architectures were carried out. The production sample prepared at lower reaction temperature 50°C consists of amorphous particles with irregular form accompanied by a small part spherical-like LDH aggregates (designated by blue dotted circle with a drawing of partial enlargement, Supporting Information Figure S6a). With the enhancing of reaction temperature to 60°C, the assembled 3-D spherical structures are formed as already presented in Figure 1. Further increase of reaction temperature does not change the size of individual LDH architecture (Supporting Information Figures S6b, c). However, the characteristic XRD reflections of LDH phase strengthen for the sample prepared at reaction temperature 90°C. The operation of the Ostwald ripening process is

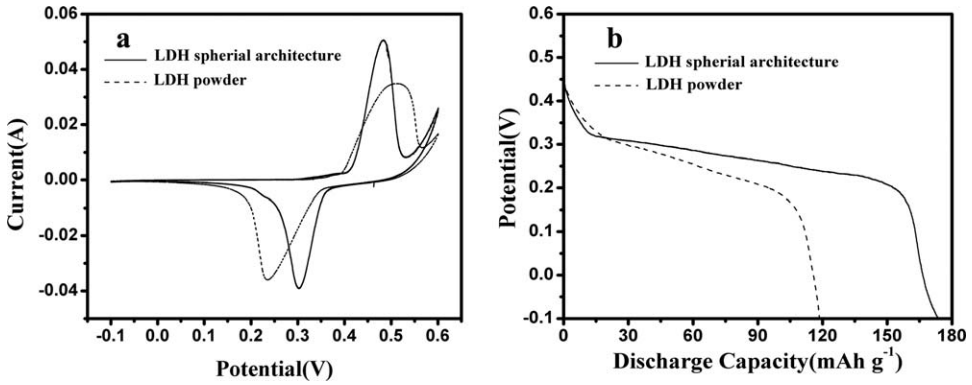

Figure 7. Electrochemical behaviors of typical sample of NiAl-LDH spherical architecture, obtained using aqueous ammonia as alkali source, and NiAl-LDH powder sample using NaOH as alkali source.

(a) Cyclic voltammograms (CVs) curves at a scan rate of 0.5 mV s^{-1}; (b) typical discharge curves as a function of capacity at a current density of 30 mA g^{-1} within a potential range from −0.1 to 0.45 V.

suggested to take place with the enhanced temperature, leading to a higher crystallinity of the LDH architecture, which was previously demonstrated by *in situ* imaging of crystal growth/dissolution of individual LDH crystals immobilized on Si substrates.[46] In addition, when we attempt the smaller aqueous ammonia dosage 5 mL at temperature 60°C, a compact aggregation of irregular or partially collapsed spherical LDH architectures is formed (Supporting Information Figure S7a). The smaller amounts of NH_3 may be inadequate under the exploited reaction conditions for complexing with Ni^{2+}, resulting in the direct nucleation of LDH in the solution. Further increase of ammonia aqueous solution, however, can produce several crystalline phases of aluminum oxide. An irregular aggregate of strip-like particles (designated by blue dotted circle) can be seen from SEM image of the sample obtained with ammonia aqueous solution 25 mL (Supporting Information Figure S7b), accompanied by the distorted LDH architectures. Meanwhile, XRD reflection in Supporting Information Figure S7b indicate the appearance of new bayerite and boehmite phase (marked by black solid arrow and black hollow arrow) and the intensity of LDH characteristic peaks decreases obviously. With a larger amount of aqueous ammonia dosage 40 mL, only mixed crystalline phases of bayerite and boehmite can be found (Supporting Information Figure S7c).

The electrochemistry properties of typical sample of NiAl-LDH spherical architecture obtained using ammonia aqueous solution (indicated in Figure 1) was further evaluated. For comparison, the data for NiAl-LDH powder obtained using NaOH (indicated in Supporting Information Figure S4b) were also measured under the identical conditions. Figure 7a shows the cyclic voltammograms of NiAl-LDH spherical architecture and NiAl-LDH powder sample. When the electrodes were scanned cathodically, two peaks, that is, the oxidation potential E_O and the oxygen-evolution potential E_{OE}, appeared. Although, during the following anodic polarization, only one peak, the reduction potential E_R was observed. The difference between the oxidation potential and the reduction potential, $E_O - E_R$, is taken as a measure of the reversibility of the electrode reaction. Table 1 demonstrates that LDH spherical architecture has the smaller $E_O - E_R$ value, demonstrating the more reversible electrode reaction. Moreover, the stronger intensities of E_O and E_R peaks is obtained for LDH spherical architecture, revealing the energy density in the spherical architecture electrode is higher than that in the powder sample. In addition, we can see that the difference value between the oxygen evolution potential and the oxidation potential, $E_{OE} - E_O$, increased from 87 mV for the powder electrode to 117 mV for the spherical architecture electrode, indicating the latter to be charged fully before oxygen evolution.[32] The above results demonstrate that the spherical architecture electrode delivers much better electrochemical-cyclic properties than the powder electrode.

Figure 7b shows the discharge curves of the spherical architecture and powder electrodes. The discharge curve of the former displays a higher discharge voltage and a longer plateau than that of the latter. The highest discharge capacity of 173 and 118 mAh g^{-1} are obtained for the spherical architecture and powder electrodes, respectively. According to the literatures, the morphology features of the electrode materials with a higher proton diffusion coefficient have been emphasized to have a very important effect on the improvement of electrochemical behavior.[31,32] Compared with LDH powder sample, LDH spherical architecture obtained using ammonia shows a larger specific surface area (Supporting Information Figure S8 and Table S1). It is noted that the LDH sphere from ammonia exhibits a narrow pore-size distribution around 3–5 nm, whereas the powder sample displays a wider pore-size distribution. Thus, the large specific area and abundant mesopores in the spherical structure promise the direct contact of the increasing electrochemical-active Ni sites with electrolyte and provide the shortening diffusion channels for electrolyte ions during the charge/discharge process. Recently, Luo et al. reported the electrochemical performance of an ordered mesoporous β-MnO_2, synthesized using mesoporous silica KIT-6 as a template, as a positive electrode for rechargeable lithium batteries.[47] The mesoporous β-MnO_2 electrode shows an excellent high rate discharge performance with the discharge capacity of

Table 1. The Comparison of Parameters of CVs for NiAl-LDH Spherical Architecture and NiAl-LDH Powder Samples

	Potentials (mV)[a]				
Electrode	E_R	E_O	E_{OE}	$E_O - E_R$	$E_{OE} - E_O$
Spherical architecture	301	481	598	180	117
Powder	237	514	601	277	87

[a]E_R: the reduction potential; E_O: the oxidation potential; E_{OE}: the oxygen-evolution potential.

158 mAh g^{-1} at a current rate of 0.4 mA cm^{-2}. In addition, the mesoporous MnO_2 electrode exhibits a capacity fading of no more than 0.2% per cycle, decreasing to 142 mAh g^{-1} at the 50th cycle. In the case of $LiCoO_2$ cathode material for lithium batteries, Ergang et al. prepared a macroporous $LiCoO_2$ by colloidal crystal templating method with a poly(-methylmethacrylate) sphere template and a precursor containing lithium acetate/cobalt acetate mixtures and evaluated its high rate capability in comparison with bulk $LiCoO_2$. Although the bulk $LiCoO_2$ electrode material shows the highest initial specific capacity of 136 mAh g^{-1} and maintains the greatest cycling stability at a relatively low rate of 27.2 mA g^{-1}, the macroporous electrode exhibits marked improvement in specific discharge capacities at higher cycling rates relative to the bulk material.[48] The above electrochemical test results (Figure 7 and Table 1) show that the hierarchical configuration of NiAl-LDH spherical architecture, which may permits diffusion and oxidation/reduction to occur easily, ensures an improved rechargeable and discharge capacity in comparison to that of NiAl-LDH powder. Further electrochemical tests of other NiAl-LDH spheres obtained with different experimental conditions are currently under investigation.

Conclusions

NiAl-LDH spherical architectures were facilely fabricated by precipitation reaction in aqueous solution containing aluminum and nickel acetate and ammonia aqueous solution as alkali source, without any surfactants and organic solvents. The obtained LDH architecture is composed of hydrotalcite-like nanoflakes with small spherical particle size of about 200 nm, high specific surface area 284 m^2 g^{-1}, and mesoporous distribution 3–5 nm. The formation process, such as the evolution of phase composition, structure, and particle morphology during the whole process was verified, which illustrates that the growth of such unique hierarchical architecture undergoes the preorganization of primary nanospheres of colloidal AAH in solution, the complexing between Ni^{2+} and NH_3 and deposition the production $Ni(NH_3)_6{}^{2+}$ compounds on the AAH surface, the conversion of Ni^{2+} and aluminum species to NiAl-LDH nuclei, the *in situ* crystallization and growth of NiAl-LDH from the exterior to the interior of AAH spheres. The structure and morphology of the LDH spherical architectures depend on both the starting raw materials and synthetic parameters such as reaction temperature and aqueous ammonia dosage. Our work demonstrates that the *in situ* transformation from the preorganized primary nanospheres of colloidal AAH would be an effective, surfactant-free, promising approach for fabricating LDH spherical architectures with size in nanometer scale in a single step. Moreover, the electrochemical performance of the obtained NiAl-LDH spherical architectures is tested as an example of their practical applications. In comparison to the NiAl-LDH powder, the spherical architecture as positive electrode material exhibits improved rechargeable and discharge capacity due to the faster diffusion processes in the hierarchical configuration of the LDH spherical architecture, suggesting the high potential as electrode material for further energy storage/conversion devices.

Acknowledgment

This work was supported by the National Natural Science Foundation of China (No. 20976006, No. 21376019), the Program for Changjiang Scholars and Innovative Research Team in University (No. IRT1205), and the 973 Program (No. 2011CBA00506).

Literature Cited

1. Whitesides GM, Grzybowski B. Self-assembly at all scales. *Science*. 2002;295:2418–2421.
2. Philp D, Stoddart JF. Self-assembly in natural and unnatural systems. *Angew Chem Int Ed*. 1996;35:1154–1196.
3. Tirrell M. Modular materials by self-assembly. *AIChE J*. 2005;51:2386–2390.
4. Stephanopoulos N, Solis EO, Stephanopoulos G. Nanoscale process systems engineering: toward molecular factories, synthetic cells, and adaptive devices. *AIChE J*. 2005;51:1858–1869.
5. Xu L, Ma W, Wang L, Xu C, Kuang H, Kotov NA. Nanoparticle assemblies: dimensional transformation of nanomaterials and scalability. *Chem Soc Rev*. 2013;42:3114–3126.
6. Zeng HC. Synthetic architecture of interior space for inorganic nanostructures. *J Mater Chem*. 2006;16:649–662.
7. Li C, Shi G. Three-dimensional graphene architectures. *Nanoscale*. 2012;4:5549–5563.
8. Shen Y, Zhan Y, Tang J, Xu P, Johnson PA, Radosz M, Van Kirk EA, Murdoch WJ. Multifunctioning pH-responsive nanoparticles from hierarchical self-assembly of polymer brush for cancer drug delivery. *AIChE J*. 2008;54:2979–2989.
9. Tang ZY, Kotov NA, Giersig M. Spontaneous organization of single CdTe nanoparticles into luminescent nanowires. *Science*. 2002;297:237–240.
10. Ding T, Song K, Clays K, Tung CH. Fabrication of 3D photonic crystals of ellipsoids: convective self-assembly in magnetic field. *Adv Mater*. 2009;21:1936–1940.
11. Wang LB, Zhu YY, Xu LG, Chen W, Kuang H, Liu LQ, Agarwal A, Xu CL, Kotov NA. Side-by-side and end-to-end gold nanorod assemblies for environmental toxin sensing. *Angew Chem Int Ed Engl*. 2010;49:5472–5475.
12. Dabbousi B, Murray C, Rubner M, Bawendi M. Langmuir-Blodgett manipulation of size-selected CdSe nanocrystallites. *Chem Mater*. 1994;6:216–219.
13. Arizaga GGC, Satyanarayana KG, Wypych F. Layered hydroxide salts: synthesis, properties and potential applications. *Solid State Ionics*. 2007;178:1143–1162.
14. Williams GR, O'Hare D. Towards understanding, control and application of layered double hydroxide chemistry. *J Mater Chem*. 2006;16:3065–3074.
15. Mousty C, Leroux F. LDHs as electrode materials for electrochemical detection and energy storage: supercapacitor, battery and (bio)-sensor. *Recent Pat Nanotechnol*. 2012;6:174–192.
16. Gao L, Xue Q, Liu Y, Lu Y. Base-free catalytic aerobic oxidation of mercaptans for gasoline sweetening over HTLcs-derived CuZnAl catalyst. *AIChE J*. 2009;55:3214–3220.
17. Yan D, Lu J, Ma J, Wei M, Evans DG, Duan X. Fabrication of an anionic polythiophene/layered double hydroxide ultrathin film showing red luminescence and reversible pH photoresponse. *AIChE J*. 2011;57:1926–1935.
18. Xu J, Gai SL, He F, Niu N, Gao P, Chen YJ, Yang PP. A sandwich-type three-dimensional layered double hydroxide nanosheet array/graphene composite: fabrication and high supercapacitor performance. *J Mater Chem A*. 2014;2:1022–1031.
19. Gunawan P, Xu R. Synthesis of unusual coral-like layered double hydroxide microspheres in a nonaqueous polar solvent/surfactant system. *J Mater Chem*. 2008;18:2112–2120.
20. Li B, He J. Multiple effects of dodecanesulfonate in the crystal growth control and morphosynthesis of layered double hydroxides. *J Phys Chem C*. 2008;112:10909–10917.
21. Prevot V, Caperaa N, Taviot-Gueho C, Forano C. Glycine-assisted hydrothermal synthesis of NiAl-lLayered double hydroxide nanostructures. *Cryst Growth Des*. 2009;9:3646–3654.
22. Wang H, Fan G, Zheng C, Xiang X, Li F. Facile sodium alginate assisted assembly of Ni-Al layered double hydroxide nanostructures. *Ind Eng Chem Res*. 2010;49:2759–2767.
23. Sun L, Hu C. Facile synthesis via a solvothermal route and characterization of Mg-Al layered double hydroxide (LDH) 3D micro-nano structures. *Mater Res Bull*. 2011;46:1922–1927.
24. Shao M, Ning F, Zhao J, Wei M, Evans DG, Duan X. Hierarchical layered double hydroxide microspheres with largely enhanced performance for ethanol electrooxidation. *Adv Funct Mater*. 2013;23:3513−3518.

25. Kang K, Meng YS, Bréger J, Grey CP, Ceder G. Electrodes with high power and high capacity for rechargeable Li batteries. *Science*. 2006;311:977–980.
26. Linden D, Reddy TB. *Handbook of Batteries*, 3rd ed. New York: McGraw-Hill, 2002.
27. Kamath PV, Dixit M, Indira L, Shukla AK, Kumar VG, Munichandraiah N. Stabilized α-Ni(OH)2 as electrode material for alkaline secondary cells. *J Electrochem Soc*. 1994;141:2956–2959.
28. Liu B, Wang XY, Yuan HT, Zhang YS, Song DY, Zhou ZX. Physical and electrochemical characteristics of aluminium-substituted nickel hydroxide. *J Appl Electrochem*. 1999;29:855–860.
29. Hu M, Gao XR, Lei LX, Sun YM. Behavior of a layered double hydroxide under high current density charge and discharge cycles. *J Phys Chem C*. 2009;113:7448–7455.
30. Mavis B, Akinc M. Three-component layer double hydroxides by urea precipitation: structural stability and electrochemistry. *J Power Sources*. 2004;134:308–317.
31. Wang XY, Luo H, Parkhutik PV, Millan AC, Matveeva E. Studies of the performance of nanostructural multiphase nickel hydroxide. *J Power Sources*. 2003;115:153–160.
32. Cai FS, Zhang GY, Chen J, Gou XL, Liu HK, Dou SX. $Ni(OH)_2$ tubes with mesoscale dimensions as positive-electrode materials of alkaline rechargeable batteries. *Angew Chem Int Ed Engl*. 2004;43:4212–4216.
33. Prevot V, Briois V, Cellier J, Forano C, Leroux F. An in-situ investigation of LDH-acetate prepared in polyol, under moderate thermal treatment. *J Phys Chem Solids*. 2008;69:1091–1094.
34. Prevot V, Forano C, Besse JP. Hydrolysis in polyol: new route for hybrid-layered double hydroxides preparation. *Chem Mater*. 2005;17:6695–6701.
35. Faour A, Mousty C, Prevot V, Devouard B, De Roy A, Bordet P, Elkaim E, Taviot-Gueho C. Correlation among structure, microstructure, and electrochemical properties of NiAl-CO3 layered double hydroxide thin films. *J Phys Chem C*. 2012;116:15646–15659.
36. Bishop KJ, Wilmer CE, Soh S, Grzybowski BA. Nanoscale forces and their uses in self-assembly. *Small*. 2009;5:1600–1630.
37. Prodromou K, Pavlatou-Ve A. Formation of aluminum hydroxides as influenced by aluminum salts and bases. *Clays Clay Miner*. 1995;43:111–115.
38. Persson P, Karlsson M, Öhman L-O. Coordination of acetate to Al (III) in aqueous solution and at the water-aluminum hydroxide interface: a potentiometric and attenuated total reflectance FTIR study. *Geochim Cosmochim Acta*. 1998;62:3657–3668.
39. Lou XW, Wang Y, Yuan C, Lee JY, Archer LA. Template-free synthesis of SnO2 hollow nanostructures with high lithium storage capacity. *Adv Mater*. 2006;18:2325–2329.
40. Yu J, Guo H, Davis SA, Mann S. Fabrication of hollow inorganic microspheres by chemically induced self-transformation. *Adv Funct Mater*. 2006;16:2035–2041.
41. Yu J, Yu H, Guo H, Li M, Mann S. Spontaneous formation of a tungsten trioxide sphere-in-shell superstructure by chemically induced self-transformation. *Small*. 2008;4:87–91.
42. Cai W, Yu J, Mann S. Template-free hydrothermal fabrication of hierarchically organized γ-AlOOH hollow microspheres. *Microporous Mesoporous Mater*. 2009;122:42–47.
43. Kloprogge JT, Duong LV, Wood BJ, Frost RL. XPS study of the major minerals in bauxite: gibbsite, bayerite and (pseudo-) boehmite. *J Colloid Interface Sci*. 2006;296:572–576.
44. Wang H, Xiang X, Li F. Facile synthesis and novel electrocatalytic performance of nanostructured Ni-Al layered double hydroxide/carbon nanotube composites. *J Mater Chem*. 2010;20:3944–3952.
45. Voegelin A, Kretzschmar R. Formation and dissolution of single and mixed Zn and Ni precipitates in soil: evidence from column experiments and extended X-ray absorption fine structure spectroscopy. *Environ Sci Technol*. 2005;39:5311–5318.
46. Greenwell H, Bindley L, Unwin P, Holliman P, Jones W, Coveney P, Barnes S. In situ monitoring of crystal growth and dissolution of oriented layered double hydroxide crystals immobilized on silicon. *J Cryst Growth*. 2006;294:53–59.
47. Luo JY, Zhang JJ, Xia YY. Highly electrochemical reaction of lithium in the ordered mesoporosus β-MnO2. *Chem Mater*. 2006;18:5618–5623.
48. Ergang NS, Lytle JC, Yan HW, Stein A. Effect of a macropore structure on cycling rates of $LiCoO_2$. *J Electrochem Soc*. 2005;152:A1989–A1995.

Manuscript received Mar. 19, 2014, and revision received Aug. 19, 2014.